Materials Science and Engineering A 528 (2011) 7933–7937

Contents lists available at ScienceDirect

Materials Science and Engineering A

journal homepage: www.elsevier.com/locate/msea

Graphene–aluminum nanocomposites

Stephen F. Bartolucci[a,*], Joseph Paras[a], Mohammad A. Rafiee[b], Javad Rafiee[c], Sabrina Lee[a], Deepak Kapoor[a], Nikhil Koratkar[c,**]

[a] U.S. Army Benét Laboratories, Armaments Research Development and Engineering Center, Watervliet, NY 12189-4000, USA
[b] Department of Mechanical Engineering and Materials Science, Rice University, Houston, TX 77005, USA
[c] Department of Mechanical, Aerospace and Nuclear Engineering, Rensselaer Polytechnic Institute, Troy, New York 12180, USA

ARTICLE INFO

Article history:
Received 22 February 2011
Received in revised form 11 July 2011
Accepted 22 July 2011
Available online 29 July 2011

Keywords:
Graphene
Carbon nanotubes
Metal–matrix composite
Mechanical properties
Powder processing

ABSTRACT

Composites of graphene platelets and powdered aluminum were made using ball milling, hot isostatic pressing and extrusion. The mechanical properties and microstructure were studied using hardness and tensile tests, as well as electron microscopy, X-ray diffraction and differential scanning calorimetry. Compared to the pure aluminum and multi-walled carbon nanotube composites, the graphene–aluminum composite showed decreased strength and hardness. This is explained in the context of enhanced aluminum carbide formation with the graphene filler.

Published by Elsevier B.V.

1. Introduction

Graphene has attracted considerable attention in the last several years because of properties such as high mechanical strength and modulus, electrical and thermal conductivity and optical transmittance. Fabrication methods have been devised to create single layer and multilayer graphene and graphene oxide in small quantities, with the intent to find methods that will result in bulk quantities of graphene for use in applications such as composites. There have been a limited amount of studies on the behavior of graphene composites. While studies have primarily been concerned with enhancing the properties of polymer matrices [1–5], with some results having shown great promise, there has been little to no research in metal matrices. This is likely a result of the greater difficulties in dispersion and fabrication, and the unknown interfacial chemical reactions in metal composites. This disparity in the amount of research given to polymer matrices as compared to metal matrices is seen in carbon nanotube (CNT) composites as well.

Aluminum has been a common material to study in metal–carbon nanotube composites due to the diverse range of technical applications for lightweight alloys. Researchers have seen mixed results with some reporting little or no increase in mechanical strength [6] while others have seen significant increases in strength. Many of these differences are a result of the quality of dispersion, fabrication method, and interfacial reactions that occur. In this study, graphene platelets derived from graphite oxide are combined with aluminum in order to observe the effects on mechanical strength.

2. Experimental procedure

Valimet H-10 atomized pure aluminum powder with an average particle size of ~22 μm was used in this study. Graphite oxide was prepared by oxidizing graphite in a solution of sulfuric acid, nitric acid, and potassium chlorate for 96 h [7,8]. Thermal exfoliation of graphite oxide was achieved by placing the graphite oxide powder in a quartz tube that was sealed at one end. The other end was closed using a rubber stopper and an argon inlet was inserted into the stopper. The sample was flushed with argon for ~10 min, and the quartz tube was quickly inserted into the tube furnace preheated to ~1050 °C and held in the furnace for ~30 s. This process exfoliates the graphite oxide into graphene platelets and removes a large portion of the oxygen groups attached to the graphene sheets [7,8]. The graphene platelets created tend to be ~3–4 carbon sheets thick and several micrometers in diameter.

Carbon vapor deposition (CVD) grown multi-walled carbon nanotubes (MWNT) from NanoLab with ~15 nm diameter, ~15–20 μm length, and 95% purity were used to make the nanotube samples.

* Corresponding author. Tel.: +1 518 266 5189; fax: +1 518 266 5161.
** Corresponding author. Tel.: +1 518 276 2630; fax: +1 518 266 2623.
E-mail addresses: stephen.bartolucci@us.army.mil (S.F. Bartolucci), koratn@rpi.edu (N. Koratkar).

0921-5093/$ – see front matter. Published by Elsevier B.V.
doi:10.1016/j.msea.2011.07.043

Table 1
Vickers hardness data for the various materials and conditions.

Material	Condition	Vickers hardness
Pure Al	As-pressed	83 ± 9
	As-extruded	96 ± 7
Al–1.0 wt% MWNT	As-pressed	102 ± 4
	As-extruded	102 ± 1
Al–0.1 wt% graphene	As-pressed	99 ± 5
	As-extruded	84 ± 5

2.1. Composite preparation

To prepare the composites, the powders were blended, milled, pressed and extruded. Aluminum–graphene composite powders were fabricated by initially blending the constituent precursory powders of Valimet Al and graphene. Blending was conducted using a Resodyn LabRAM acoustic mixer for ~5 min. This blend was then milled in a Zoz high energy attritor under an Argon atmosphere for one hour. Stearic acid (2 wt%) was used as a process control agent to prevent agglomerations. In addition to creating a homogenous composite powder, the milling cycle also imparts some degree of grain refinement and breaks the nascent oxide layer off of the aluminum, providing a clean metallurgical interface. This clean interface aided the consolidation process performed via instrumented hot isostatic pressing (I-HIP), uniquely equipped with a High Temperature Eddy Current Sensor (HiTECS) to monitor, in real-time, the densification of the composite powder. HIP conditions were tailored for each sample using the HiTECS, but processing was typically done at ~375 °C for ~20 min. All samples were near 100% of the theoretical density as measured by the Archimedes method. Samples of pure aluminum, 0.1 wt% graphene and 1.0 wt% MWNT were made. Dispersion of graphene is more challenging as compared to carbon nanotubes due to their greater interfacial contact area [4] and hence a low weight fraction of graphene was chosen for this test.

After hot isostatic pressing, the ~20 mm diameter billets were preheated to ~550 °C for ~4 h and then extruded on a 50-ton aluminum extrusion press. The extrusion ratio was 4:1, ram speed was ~12.5 mm/s, and extrusion pressure reached ~65 ksi. Pure aluminum, Al–graphene, and Al–MWNT samples were all prepared in the same manner.

2.2. Characterization

Vickers hardness tests were performed on the materials with a 200 g weight. A minimum of 5 data points were averaged for each material. Materials were machined into flat dog-bone tensile coupons and tested with a ~0.5 mm/min crosshead rate on an Instron tensile testing machine. The tensile properties reported were the calculated average of 3 samples. Microstructural observations were also performed by field-emission scanning electron microscopy (FE-SEM) on a JEOL 6330F operating at 5 kV.

The structure of the Al, Al–graphene, and Al–MWNT samples were examined using a Scintag 4-circle PTS Diffractomer; using K-alpha radiations from a fine-focus Cu X-ray tube. X-ray diffraction (XRD) scans were obtained for two-theta range 5–90° at ~0.1° step, ~10 s/point. Total XRD scan took ~2.5 h per scan.

Differential Scanning Calorimetry (DSC) was performed on a Perkin-Elmer DSC 7 and heated at ~10 °K/min for the steady heating experiments and ~20 °K/min for the isothermal experiments.

3. Results and discussion

Table 1 shows the hardness of the various samples after hot isostatic pressing and after extrusion. It is clear from the data that the aluminum reinforced with 1.0 wt% MWNT displays the highest hardness among the materials tested. Pure aluminum showed an increase in hardness after extrusion to a value slightly below the nanotube reinforced material. The increase in hardness is likely due to the formation of a more refined and compacted microstructure. The graphene composite showed high as-pressed hardness, but then exhibited a marked decrease in its hardness after extrusion. Fig. 1a shows the tensile strengths of the extruded materials. The nanotube sample had the highest strength and the graphene sample showed the lowest tensile strength. The tensile strength of the nanotube composite was ~12% greater than the baseline, while the graphene composite showed ~18% lower tensile strength as compared to the baseline aluminum. Fig. 1b shows the average strain-to-failure of the samples. The nanotube and graphene samples displayed the lowest ductility. The observed decrease in ductility, as we see in our results for the nanotube composites, has been widely reported in the work of others. The pure aluminum and the 1.0 wt% MWNT had average 0.2% offset yield strengths of 300 MPa and 297 MPa, respectively, while the graphene sample had an average Y.S. of 198 MPa.

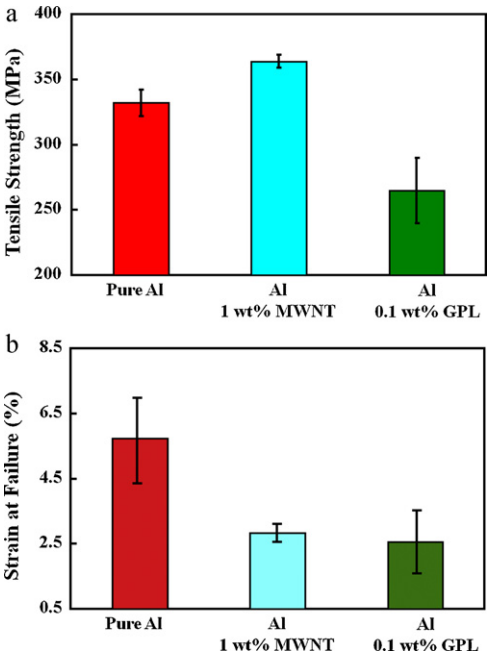

Fig. 1. (a) Ultimate tensile strengths of pure Al, Al–1 wt% MWNT, and Al–0.1 wt% graphene and (b) strain-to-failure.

XRD scans for the Al, Al–0.1 wt% graphene, and the 1.0 wt% MWNT are shown in Fig. 2. All samples have major aluminum peaks

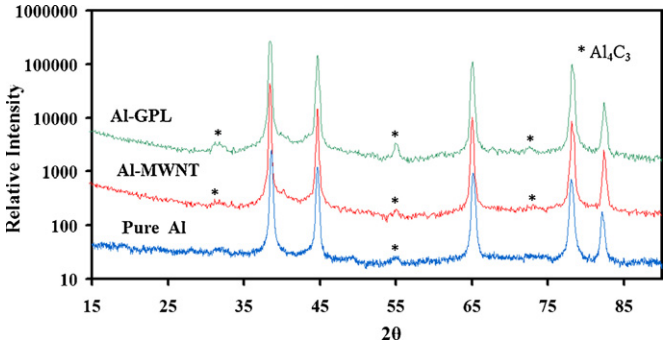

Fig. 2. X-ray diffraction of pure aluminum, Al–1.0 wt% MWNT composite, and Al–0.1 wt% graphene composite after extrusion.

at ~38.3° (1 1 1), ~44.6° (2 0 0), ~65.1° (2 2 0), ~78.2° (3 1 1) and ~82.3° (2 2 2). Despite only having ~0.1 wt% graphene filler in the Al–graphene composite, strong peaks for aluminum carbide (Al_4C_3) are seen at ~31.2° and ~31.8°, ~55.0°, and ~72.5° two theta. Less intense peaks are seen in the other two samples. There may be some carbide that forms, even in the pure aluminum, from stearic acid/organics that may not have been fully removed before HIP'ing [9]. The graphene composite has the strongest peaks for Al_4C_3 among all the samples.

3.1. Carbide formation

Aluminum carbide, Al_4C_3, which is the most energetically favorable stoichiometry of the aluminum carbides to form at the temperatures of interest in this study [10], will grow on the high surface free energy prismatic planes of carbon. This has been seen in conventional sized carbon fibers and is deleterious to the strength of the composite [11,12]. The highly stable defect-free graphitic planes of the carbon nanotube or graphene do not react with aluminum to form aluminum carbide even at very high temperatures when the aluminum is liquid. Carbide formation will be promoted at defects in the graphitic planes (which exposes the prism planes), at tubes ends, and amorphous carbon coating at temperatures below the aluminum melting point [13]. Because of the complex conditions that lead to the growth or suppression of the aluminum carbide phase, some authors have reported the formation of Al_4C_3 [13–17], while others have not observed its formation [6,18,19]. It is interesting to note that those who have observed the aluminum carbide phase [13,16,17] in the Al–MWNT composites used CVD grown carbon nanotubes. It is known that CVD grown CNT have a higher density of defects along the outer walls. Previous work that did not report observing Al_4C_3 used arc-discharge grown CNTs [6,19], which are known to have high quality, defect free outer graphitic walls.

The materials in this study have been exposed to ~375 °C for ~20 min during the HIP'ing process and ~550 °C for ~4 h during extrusion preheat. A temperature rise can be expected during extrusion due to deformational and frictional heating, but it is likely to be less than ~50 °C and only occurs for a short amount of time. Previous results that have reported the presence of Al_4C_3 in the composite had processing temperatures that were above 500 °C. Deng et al. [17], did not see Al_4C_3 in the composite extruded at ~460 °C, but did see it form in differential scanning calorimetry (DSC) experiments above ~672 °C. Kwon et al. [16], observed carbide in samples heat treated at ~500 °C for 2 h and then spark plasma sintered (SPS) at temperatures between 480 and 600 °C. Ci et al. [13], report observing Al_4C_3 formation in CVD MWNT-sputtered aluminum composites after annealing at 500 °C and above. XRD on 400 °C annealed composites did not show any carbide peaks.

The graphene platelets used in this research were produced by thermal reduction of graphite oxide. This processing results in graphene that has a wrinkled morphology and defects on the graphitic basal plane [4,7]. This can be seen in the TEM micrograph in Fig. 3a. The abundance of defect sites is also confirmed by Raman spectroscopy. Raman analysis (Fig. 3b) of the graphene powder indicated an intense D band and significant broadening of both the D and G bands indicating a high degree of disorder. This high defect density is an artifact of the oxidation of graphite and the thermal shock technique that was employed to exfoliate graphite oxide to graphene platelets. The defects expose the prism planes of the graphene, which can become reaction sites with the aluminum. The abundant amount of prism planes at the graphene platelet edges could also become reaction sites. This could result in significant amounts of Al_4C_3 when compared to the total volume fraction of graphene since the graphene sheets are only on the order of a few atomic layers thick. This may result in the lower mechanical strength that we see for the graphene samples.

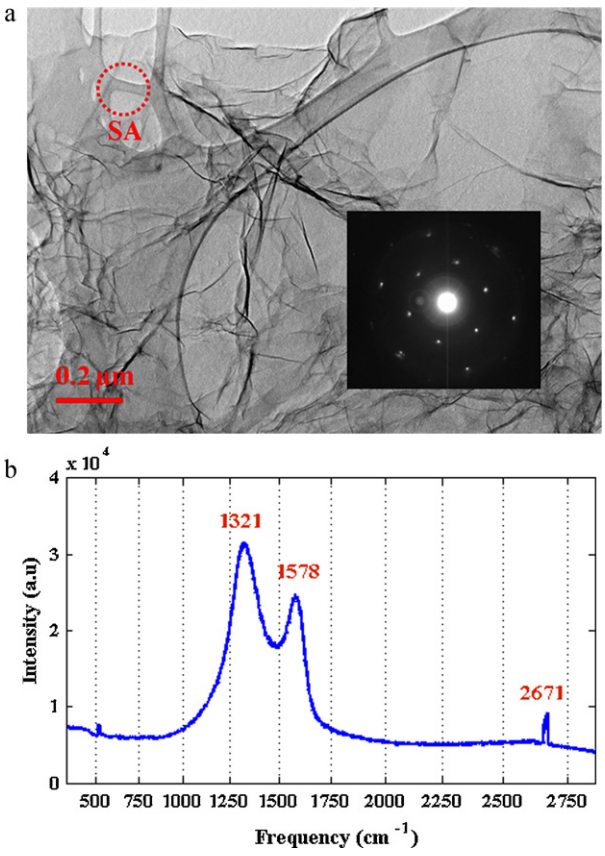

Fig. 3. (a) Transmission Electron Micrograph of graphene platelet showing the wrinkled morphology. Inset shows the selected area diffraction pattern (SADP) of the hexagonal graphene cell. (b) For Raman analysis, the graphene platelets were deposited on silicon wafers in powder form without using any solvent. Raman spectra of the samples were measured using a micro-spectrometer using an excitation wavelength of ~785 nm. The Raman G, D and 2D band peaks are observed at ~1578 cm^{-1}, ~1321 cm^{-1} and ~2671 cm^{-1}, respectively. Note that the D band peak is higher in intensity than the G band and both peaks are significantly broadened which suggests a high density of defects in the graphene platelets.

3.2. Differential Scanning Calorimetry

DSC studies were conducted on the materials in order to detect phase transformations such as the formation of the aluminum carbide. The DSC results are shown in Fig. 4. The DSC curves did not show any clear transformations occurring as the samples were heated to 700 °C, except for the large endothermic peak during melting around 676 °C (with a slight depression of the melting point for the graphene sample). A second DSC run was performed where the samples were heated to 550 °C and held for 1hr. This test simulated the 550 °C hold during extrusion preheat (preheat was actually 4 h). However, these curves also did not show any significant differences between the pure aluminum and the aluminum–graphene sample. Others that have reported DSC studies on aluminum with ~5 wt% CNTs in Al-2024 observed exothermic peaks after melting, indicative of aluminum carbide formation [15,17]. Since our samples contain a comparatively very small amount (~0.1% by weight) of graphene, our calculations have shown it is likely under the resolution of the DSC to record the carbide formation.

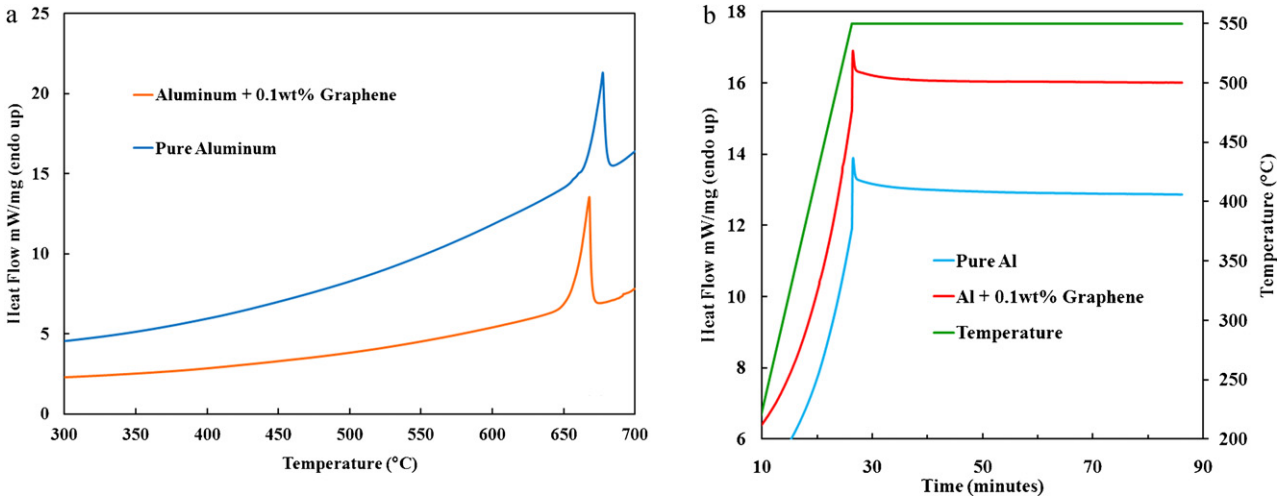

Fig. 4. Differential Scanning Calorimetry of aluminum and aluminum–graphene composites. (a) Linear heating to 700 °C, (b) isothermal hold at 550 °C.

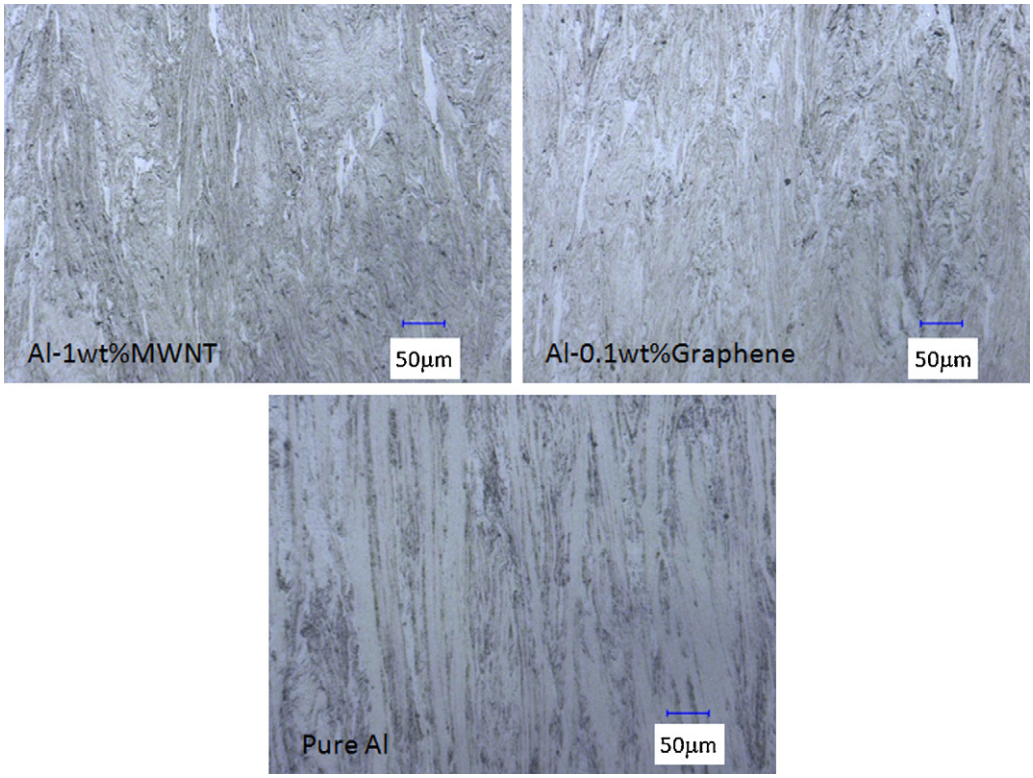

Fig. 5. Optical micrographs of extruded Al–1 wt% MWNT, Al–0.1 wt% graphene, and pure Al.

3.3. Microstructure

Fig. 5 shows micrographs of polished and etched (Keller's etch) aluminum, aluminum–MWNT and aluminum–graphene samples in the extruded condition. The microstructure shows the retained structure from powder consolidation and alignment during extrusion. Because of this microstructure, it is very difficult to make a quantitative measurement on grain size. It has been reported that nano-additives can inhibit grain growth through grain boundary pinning [17] and therefore lead to a finer grain structure. Finer grain structures can result in higher hardness values. Although all three materials display fine grain structure, it could be argued that the pure aluminum has a slightly coarser structure than the nanocomposites. This could contribute to the nanocomposites having higher as-pressed hardness values. It should be noted that the as-pressed microstructures were comparable to the extruded microstructures shown in Fig. 5, but without the alignment in the extrusion direction. Despite what could be a finer microstructure than the pure aluminum, the apparent formation of aluminum carbide in the graphene nanocomposite still leads to a deleterious effects on tensile properties.

Graphene may adhere to the surface of the aluminum particles during milling, as we have seen previously with carbon nanotubes. During consolidation, and subsequent heating and extrusion, the graphene may react with the aluminum on these grain boundaries to form aluminum carbide. These may then become points of brittle weakness leading to decreased mechanical properties.

Graphene may still prove to be a promising reinforcement agent for metals, especially those that do not form a carbide, or ones in which very little carbide is formed. In this sense, the graphene could form reinforcing particles that could add strength to the composite in the same way that finely dispersed second phase precipitates do in precipitation hardened aluminum alloys. It may be difficult to process graphene–aluminum composites with good mechanical properties unless careful attention is given to the processing temperatures in order to avoid the formation of aluminum carbide.

4. Conclusions

We have fabricated aluminum nanocomposites by milling, hot isostatic pressing, and hot extrusion. Our results indicate that multiwalled carbon nanotubes can increase the tensile strength of aluminum by up to ~12%. However we find that graphene is prone to forming aluminum carbide during processing, which lowers the hardness and tensile strength of aluminum. The defective nature of graphene produced by thermal exfoliation/reduction of graphite oxide is likely responsible for promoting aluminum carbide formation. While defects in graphene has been shown to enhance interfacial binding and load transfer with polymer matrices [1,2,4], the same is not true for aluminum matrices.

Acknowledgments

The authors wish to acknowledge Prof. Roger N. Wright at Rensselaer Polytechnic Institute for his assistance in extruding the aluminum billets.

References

[1] M.A. Rafiee, J. Rafiee, Z.-Z. Yu, N. Koratkar, Appl. Phys. Lett. 95 (2009) 223103.
[2] M.A. Rafiee, J. Rafiee, H. Song, Z.-Z. Yu, N. Koratkar, ACS Nano. 3 (12) (2009) 3884–3890.
[3] M.A. Rafiee, W. Lu, A.V. Thomas, A. Zandiatashbar, J. Raviee, J. Tour, N. Koratkar, ACS Nano. 4 (12) (2010) 7415–7420.
[4] M. Rafiee, J. Rafiee, I. Srivastava, Z. Wang, H. Song, Z.-Z. Yu, N. Koratkar, Small 6 (2010) 179–183.
[5] Y. Zhu, S. Murali, W. Cai, X. Li, J.W. Suk, J.R. Potts, R.S. Ruoff, Adv. Mater. 22 (2010) 3906–3924.
[6] T. Kuzumaki, J. Mater. Res. 13 (September (9)) (1998) 2445–2449.
[7] H.C. Schniepp, J.-L. Li, M.J. McAllister, H. Sai, M. Herrera-Alonso, D.H. Adamson, R.K. Prud'homme, R. Car, D.A. Saville, I.A. Aksay, J. Phys. Chem. B 110 (2006) 8535–8539.
[8] M.J. McAllister, J.-L. Li, D.H. Adamson, H.C. Schniepp, A.A. Abdala, J. Lui, M. Herrera-Alonso, D.L. Milius, R. Car, R.K. Prud'homme, I.A. Aksay, Chem. Mater. 19 (2007) 4396–4404.
[9] C. Rubio-González, C. Felix-Martinez, G. Gomez-Rosas, J.L. Ocaña, M. Morales, J.A. Porro, Mater. Sci. Eng. A 528 (2011) 914–919.
[10] T. Laha, S. Kuchibhatla, S. Seal, W. Li, A. Agarwal, Acta Mater. 55 (2007) 1059–1066.
[11] Y. Ishida, H. Ichinose, J. Wang, T. Suga, in: G.W. Bailey, Proceedings of the 46th Annu. Met. Electr. Micros. Soc. of America, San Francisco (1988) 728.
[12] Y. Zhou, W. Yang, Y. Xia, P.K. Mallick, Mater. Sci. Eng. A 362 (2003) 112–117.
[13] L. Ci, Z. Ryu, N.Y. Jin-Phillipp, M. Ruhle, Acta Mater. 54 (2006) 5367–5375.
[14] H. Kwon, M. Estili, K. Takagi, T. Miyazaki, A. Kawasaki, Carbon 47 (2009) 570–577.
[15] C.F. Deng, X.X. Zhang, D.Z. Wang, Y.X. Ma, Mater. Lett. 61 (2007) 3221–3223.
[16] H. Kwon, D.H. Park, J.F. Silvain, A. Kawasaki, Compos. Sci. Technol. 70 (2010) 546–550.
[17] C.F. Deng, D.Z. Wang, X.X. Zhang, A.B. Li, Mater. Sci. Eng. A 444 (2007) 138–145.
[18] R. Pérez Bustamante, I. Estrada-Guel, W. Antúnez-Flores, M. Miki-Yoshida, P.J. Ferreira, R. Martínez-Sánchez, J. Alloys Compounds 450 (2008) 323–326.
[19] R. George, K.T. Kashyap, R. Rahul, S. Yamdagni, Scr. Mater. 53 (2005) 1159–1163.